

Instabilities induced by concentration gradients in dusty gases

By JUAN A. HERNÁNDEZ¹

¹School of Aeronautics, U. Politécnica, 28040-Madrid, Spain

(Received 17 June 1999 and in revised form 27 November 2000)

This paper deals with the stability of suspensions modelled as dusty gases for non-uniform profiles of mass fraction of particles. It is known that a stationary uniform fluidized bed may be unstable to small disturbances which grow until a secondary instability develops forming bubbles that rise through the bed. Interactions between particles are difficult to model and this makes it necessary to close the model with some assumptions. However, in dilute fluidized beds which are characterized by a low volume fraction of particles, interactions between particles are negligible and this motivates the study of instabilities of suspensions by means of the dusty gas equations, avoiding the problem of particular closures.

We show in this work that suspensions blown to regions of higher concentration are unstable to two-dimensional disturbances. An equation which governs this instability is obtained. A physical mechanism is proposed to explain this instability and it is related to the Rayleigh–Taylor one in the limit of long characteristic lengthscales associated with the concentration profile. Finally, the evolution of this instability is followed using a fully nonlinear numerical code showing the formation of streamers and clusters of particles.

1. Introduction

We are concerned in this paper with investigating the stability of suspensions of particles by means of dusty gas equations. The motivation is partly the behaviour of dilute flow encountered either in fast fluidized beds or at the free surface of a bubbling fluidized bed, and partly the desire to study the phenomenon of bed instability in a regime in which the modelling of the two-phase flow can be simplified to a great extent.

When the gas velocity in a fluidized bed is close to the minimum fluidization velocity, in which the drag of particle clusters equilibrates their weight, the bed bubbles vigorously. When the velocity is increased further, the aerodynamic drag of even single particles becomes larger than their weight, and the bed enters the fast fluidization regime. The particles are blown out of the top of the bed, and have to be recirculated externally.

These so-called fast or circulating fluidized beds are very attractive in applications in which an intimate contact of gas and solids is important. They are used in catalytic processes, and in gas–solid reactions like calcination and combustion. In general, in spite of their industrial importance, much of the knowledge of fast fluidized beds is empirical, and theoretical information is scarce. They are known to be very inhomogeneous, typically characterized by a progression from concentrated to dilute from bottom to top, with a concomitant radial segregation into a dilute core and

a more concentrated annulus toward the top (Brereton & Grace 1993; Dasgupta, Jackson & Sundaresan 1994). The spatial distribution of solids is characterized by dense strands or clusters (Yerushalmi & Cankurt 1978), which have been observed to be paraboloidal in shape, opening upwards (Horio & Kuroki 1994).

Three basic levels of modelling have commonly been applied to fluidized beds, the first two adopting the concept of interpenetrating (continuum) fluids. The third, most comprehensive, level is to endow each of the two phases with its own stress tensor, and to account explicitly for volumetric coupling (i.e. the effect of fraction of solids on the densities of both phases) along with interphase friction (Fanucci, Ness & Yen 1979; Needham & Merkin 1983; Hernández & Jiménez 1991). The stresses and friction terms pose troublesome questions for closure – whether by Reynolds-type averaging analogous to turbulence theory (Buyevich 1971; Drew 1983; Jackson 1996) or by phenomenological empiricism. Such two-fluid models have successfully predicted some known instabilities of fluidized beds (Homsy, El-Kaissy & Didwania 1980; Hernández 1990; Anderson, Sundaresan & Jackson 1995; Glasser, Kevrekidis & Sundaresan 1996). The key question is: which elements of the macroscopic closure are necessary to capture which instabilities? Volumetric coupling in the model leads to the primary instability by which a uniform concentration profile segregates into alternating horizontal layers of higher and lower density (Jackson 1963). Further work by Needham (1986), Harris & Crighton (1994) and Harris (1996), provided valuable approaches to the one-dimensional nonlinear behaviour of voidage disturbances of fluidized beds: it is believed that a secondary, two-dimensional ‘overturning’ instability grows out of these layers to form the bubbles that rise through the bed. The importance of the relative timescales of the primary versus secondary instabilities emerges from the extensive analysis of Anderson *et al.* (1995) for gas- and water-fluidized beds. Bifurcation theory reveals a universal qualitative structure independent of the particular closure approximations (Göz 1995; Glasser, Kevrekidis & Sundaresan 1997; Glasser, Sundaresan & Kevrekidis 1998).

The dusty gas equations (§2) discard volumetric coupling between the two interpenetrating phases (assuming suitably dilute solids), but retain the interphase drag. Correspondingly, the primary instability is lost from the model (§3.1), but susceptibility to the secondary instability once a horizontal stratification has formed remains. (Gradients can thus have a significant effect even under conditions where the primary instability is not important, such as low volume fraction with mass fraction of order unity.) The same is true of the even simpler one-fluid model (Batchelor & Nitsche 1991; Batchelor 1993), which applies when the slip velocity of the perturbations between the gas and the particles is small (mass fraction of solids much greater than unity). The motivation of using the dusty gas equations here is that they could apply to the dilute core region near the top of fast fluidized beds, where the one-fluid assumptions are not valid.

As well as linear stability theory (§3.1) applied to a sinusoidal variation (§3.2) and the limiting case of a step change (§3.3), this paper tracks the nonlinear evolution numerically (§4), through to the evolution of strands (mass fractions of order 10) and paraboloidal clusters (mass fractions of order unity). To our knowledge, this is the first time that the whole transition process has been computed.

2. Equations for dusty gases

Equations of dusty gases have been analysed extensively in the literature. We use the two-fluid model proposed by Saffman (1962) and used by Ishii & Matsuhisa

(1983) and Dasgupta *et al.* (1994). In these equations the phases are represented as interpenetrating fluids, each of which occupies the whole two-dimensional space. Since the volume fraction of particles is small, the interactions between particles and the volumetric coupling between phases can be neglected in the conservation equations. Each phase has its own continuity and momentum equation, and the only interaction between the phases is in the form of a mutual drag. The gas is assumed to be incompressible with a density ρ_g , and the density of the particles ρ_p is taken to be much larger than that of the gas.

In most practical cases the size of the particles is not uniform, in which case several 'fluids' may be needed to represent each size range. In this paper, the problem is simplified by considering identical particles, large enough to neglect their Brownian motion, and close enough to spherical for lift forces to be negligible.

We will further assume that the Reynolds number based on the particle diameter and on the particle–gas slip velocity is small, so that the drag force on an isolated particle obeys Stokes' law. If we assume that the slip velocity is of the order of the terminal velocity of an isolated particle $U_t = \rho_p g d^2 / (18 \mu_g)$ under the action of gravity (g), its Reynolds number can be defined as

$$Re_t = \frac{\rho_g U_t d}{\mu_g}, \quad (2.1)$$

where d is the particle diameter, and μ_g is the gas viscosity. The requirement of Re_t of order unity limits our analysis to sufficiently fine particles.

We will also suppose that the Reynolds number of the gas flow is large enough to consider the gas inviscid except for its interaction with the particles. If we assume that the gas velocity is of the order of the terminal velocity and the characteristic length of the gas flow is L_v , we can define a Reynolds number of the gas flow as

$$Re = \frac{\rho_g U_t L_v}{\mu_g}. \quad (2.2)$$

The requirement that Re be much greater than unity limits the validity of the model to sufficiently coarse particles.

For the present study we define the mass fraction of particles β as the volume fraction of particles multiplied by ρ_p/ρ_g . We consider that β is of order unity and we normalize the equations with the terminal velocity U_t , with the relaxation time $\tau_v = U_t/g$, and the viscous length derived from them $L_v = \tau_v^2 g$. The dimensionless equations of conservation of mass and momentum for the particles and the gas are

$$\frac{\partial \beta}{\partial \tilde{t}} + \nabla \cdot (\beta \tilde{\mathbf{v}}_p) = 0, \quad (2.3)$$

$$\frac{\partial \tilde{\mathbf{v}}_p}{\partial \tilde{t}} + \tilde{\mathbf{v}}_p \cdot \nabla \tilde{\mathbf{v}}_p = -\mathbf{i} + \tilde{\mathbf{v}}_g - \tilde{\mathbf{v}}_p, \quad (2.4)$$

$$\nabla \cdot \tilde{\mathbf{v}}_g = 0, \quad (2.5)$$

$$\frac{\partial \tilde{\mathbf{v}}_g}{\partial \tilde{t}} + \tilde{\mathbf{v}}_g \cdot \nabla \tilde{\mathbf{v}}_g = -\nabla \tilde{P}_g + \beta(\tilde{\mathbf{v}}_p - \tilde{\mathbf{v}}_g), \quad (2.6)$$

where $\tilde{\mathbf{v}}_p, \tilde{\mathbf{v}}_g$ are the macroscopic dimensionless velocities of the particles and gas respectively, \tilde{P}_g is the gas pressure including the hydrostatic term made dimensionless with $\rho_g U_t^2$, and \mathbf{i} is the unit vector along the x -axis, opposite to the direction of gravity.

In order to see the range of particles that we can analyse with equations (2.3)–(2.6),

d (μm)	U_t (cm s^{-1})	Re_t	L_v (cm)	τ_v (ms)	Re
70	26	1.2	0.66	26	114
100	53	3.6	2.8	53	1002
150	121	12.1	15	123	12100

TABLE 1. Parameters of the range of particles analysed.

we list in table 1 the terminal velocity and the viscous length for different diameters of particles with $\rho_p = 1.78 \text{ g cm}^{-3}$. To ensure that the drag force obeys the Stokes law, Re_t must be of order unity and, hence, particle diameters must be less than $150 \mu\text{m}$. Also, to neglect viscous stresses of the gas, Re must be much greater than unity which limits the analysis to particle diameters greater than $70 \mu\text{m}$.

We will focus our work in the behaviour of non-uniform suspensions of particles between 70 and $150 \mu\text{m}$ with associated characteristic lengths greater than 1 cm fluidized by air.

3. Linear stability analysis of dusty gases

We will consider a vertical distribution of particles under the action of gravity suspended by an upward gas flow. We will analyse the stability of the following steady solutions: a sinusoidal mass fraction distribution and a step-like distribution of particles. The step-like distribution is analysed to obtain an analytical bound of the growth rate of the instability with the most simple non-uniform distribution.

In §3.2 and §3.3 we will see how non-uniform suspensions are unstable to two-dimensional disturbances with a characteristic timescale $t = O(\tau_v)$ when they are blown to regions of higher concentration. We will explain that the physical mechanism of this instability induced by concentration gradients in the long wave limit is equivalent to the Rayleigh–Taylor instability.

3.1. The disturbance equations of a non-uniform suspension

We consider a steady solution of dusty gas equations (2.3)–(2.6) in which the initial mass fraction distribution varies with height. The only non-uniform steady solution with an arbitrary distribution of particles is a suspension at rest in which the weight of particles is equilibrated by the drag of a gas blowing upwards:

$$\beta = \gamma B(\tilde{x}), \quad \tilde{\mathbf{v}}_p = 0, \quad \tilde{\mathbf{v}}_g = \mathbf{i}, \quad \nabla \tilde{P}_0 = -\gamma B(\tilde{x})\mathbf{i}, \quad (3.1)$$

where P_0 is the gas pressure. We add an infinitesimal transversal perturbation,

$$\beta = \gamma B(\tilde{x}) + \gamma \tilde{\beta}(\tilde{x}) \exp(i\kappa_y \tilde{y} + \mu \tilde{t}), \quad \tilde{\mathbf{v}}_p = (u_p, v_p) \exp(i\kappa_y \tilde{y} + \mu \tilde{t}), \quad (3.2)$$

$$\tilde{\mathbf{v}}_g = \mathbf{i} + (u_g, v_g) \exp(i\kappa_y \tilde{y} + \mu \tilde{t}), \quad \tilde{P}_g = \tilde{P}_0 + P(x) \exp(i\kappa_y \tilde{y} + \mu \tilde{t}). \quad (3.3)$$

Here, κ_y is real and μ complex. Linearizing equations (2.3)–(2.6) around the steady state gives

$$DBu_p + \mu \tilde{\beta} + B(Du_p + i\kappa_y v_p) = 0, \quad (3.4)$$

$$\mu u_p = u_g - u_p, \quad (3.5)$$

$$\mu v_p = v_g - v_p, \quad (3.6)$$

$$Du_g + i\kappa_y v_g = 0, \quad (3.7)$$

$$\mu u_g + Du_g = -DP + \gamma B(u_p - u_g) - \gamma \tilde{\beta}, \quad (3.8)$$

$$\mu w_g + Dv_g = -i\kappa_y P + \gamma B(v_p - v_g), \quad (3.9)$$

where D stands for differentiation with respect to \tilde{x} . Since volumetric coupling between phases is neglected, the gas is considered incompressible (3.7). It is easy to prove by combining equations (3.5)–(3.7) that the particle phase is also linearly incompressible,

$$Du_p + i\kappa_y v_p = 0. \quad (3.10)$$

If now we assume $B(\tilde{x}) = O(1)$ with variations much less than unity and make the Boussinesq approximation that density variations are significant only through their influence on the gravitational force, gas pressure P can be eliminated with equations (3.8)–(3.9) to obtain an equation for the vorticity of the gas:

$$(D + \mu)\omega_g = \gamma(\omega_p - \omega_g) - i\kappa_y \gamma \tilde{\beta}, \quad (3.11)$$

where $\omega_g = Dv_g - i\kappa_y u_g$, and $\omega_p = Dv_p - i\kappa_y u_p$. The left-hand-side terms represent the convection and local variation of the vorticity of the gas, while the term $i\kappa_y \gamma \tilde{\beta}$ on the right-hand-side represents the creation of vorticity in the gas by the drag between phases. An equation for the vorticity of the particles is obtained using equations (3.5)–(3.6):

$$\mu\omega_p = \omega_g - \omega_p. \quad (3.12)$$

The variables β , u_g , v_g , v_p can be eliminated with equations (3.4) and (3.10)–(3.12) to give

$$\mu\{(D + \mu)(\mu + 1) + \gamma\mu\}(D^2 - \kappa_y^2)u_p = -\gamma\kappa_y^2 DB u_p. \quad (3.13)$$

Uniform concentration profiles ($DB = 0$) are neutrally stable. For bounded eigenfunctions $u_p(\tilde{x})$ in an infinite domain, it is easy to prove that if

$$\int_{-\infty}^{+\infty} DB u_p^2 dx > 0, \quad (3.14)$$

then there exists at least one eigenvalue with real part greater than zero. As a particular case, the condition (3.14) is fulfilled for increasing distributions with $DB(\tilde{x}) > 0$ in the whole fluid domain. Hence, particles blown up to regions of higher concentration are unstable to two-dimensional disturbances.

When considering disturbances of wavelengths much greater than the viscous length, this instability is equivalent to the Rayleigh–Taylor instability. In the long wave limit ($\kappa_y \ll 1$), particles follow closely the variations of the gas velocity, and the mixture can be considered as one phase with a new density $1 + \gamma$. Considering that $D = O(\kappa_y)$ and $DB = O(\kappa_y)$ (which is equivalent to rescaling the problem with κ_y) we can look for eigenvalues $O(\kappa_y^{1/2})$ and equation (3.13) gives

$$\mu^2(1 + \gamma)(D^2 - \kappa_y^2)u_p = -\gamma\kappa_y^2 DB u_p, \quad (3.15)$$

which is the Rayleigh–Taylor equation (Chandrasekhar 1981) for the stability of a stratified fluid with density $1 + \gamma$. However, for values of $\kappa_y = O(1)$ the full equation (3.13) must be retained.

3.2. Sinusoidal mass fraction distribution

The mass fraction of particles is written as

$$B(\tilde{x}) = 1 + \Delta \sin(\kappa_x \tilde{x}), \quad (3.16)$$

in which the constant Δ is positive. We can look for a Fourier expansion of the form

$$u_p(\tilde{x}) = \sum_{n=-\infty}^{\infty} \hat{u}_n \exp(in\kappa_x \tilde{x}), \quad (3.17)$$

where \hat{u}_n is the complex amplitude of the harmonic n . Substituting the Fourier expansion for u_p in (3.13) we obtain

$$\sum_{n=-\infty}^{\infty} G_n \hat{u}_n \exp(in\kappa_x \tilde{x}) = \sum_{n=-\infty}^{\infty} \hat{u}_n (\exp(i(n+1)\kappa_x \tilde{x}) + \exp(i(n-1)\kappa_x \tilde{x})) \quad (3.18)$$

with

$$G_n = \frac{2\mu(n^2 + A^2)}{\gamma \Delta \kappa_x A^2} \{(in\kappa_x + \mu)(\mu + 1) + \gamma\mu\}, \quad (3.19)$$

and

$$A = \frac{\kappa_y}{\kappa_x}. \quad (3.20)$$

Projecting along sines and cosines we obtain

$$G_n \hat{u}_n = \hat{u}_{n+1} + \hat{u}_{n-1}, \quad n = -\infty \dots \infty, \quad (3.21)$$

which is a homogeneous system of linear equations. Setting the determinant of the system to zero, we obtain the eigenvalues of stability. The numerical treatment of the problem requires the truncation of the expansion (3.17) with a number of harmonics great enough to give a negligible error.

The eigenvalues of stability depend on the following parameters: $\Delta, \gamma, \kappa_x, A$. To study the dependence of the stability on these parameters we plot in figure 1 μ versus A for two different values of mass fraction γ . In figure 1(a) $\gamma = 1$ and different values of κ_x are plotted to show the influence of the characteristic length of the concentration gradient $L_x = 2\pi L_y / \kappa_x$. We note that there is no mechanism to stabilize the short wavelength ($\kappa_x \gg 1$) but the growth rate of the instability is bounded. Also, there is a transversal wavelength $L_y = O(L_x)$ for which the instability has a maximum growth rate. The behaviour in figure 1(b) for mass fraction $\gamma = 10$ is similar than for $\gamma = 1$ but the bound of the growth rate is reached for small values of L_x . It is important to note that while in the Rayleigh–Taylor instability predicted by equation (3.15) the most unstable transversal disturbance κ_y corresponds to the shortest wavelength present, the most unstable transversal disturbance predicted by equation (3.13) is achieved for a finite value of $\kappa_y = O(\kappa_x)$.

For particles of $70 \mu\text{m}$ and mass fractions of order unity, this instability will be significant for concentration gradients with a characteristic wavelength $L_x \approx 4 \text{ cm}$ and the maximum growth rate will be achieved for transversal wavelength $L_y \approx 2 \text{ cm}$ with a characteristic evolution time $t \approx 0.2 \text{ s}$. For particles of $150 \mu\text{m}$ and mass fractions of order unity, this instability will be significant for concentration gradients with a characteristic wavelength $L_x \approx 90 \text{ cm}$ and the maximum growth rate will be achieved for transversal wavelength $L_y \approx 55 \text{ cm}$ with a characteristic evolution time $t \approx 0.8 \text{ s}$.

3.3. Step-like mass fraction distribution

As we have seen, the maximum growth rate of the instability of a concentration gradient is bounded. In this section we will obtain an analytical bound for the growth rate of the instability. The stability of disturbances is governed by (3.13). This equation is especially easy to analyse if the undisturbed mass fraction distribution is

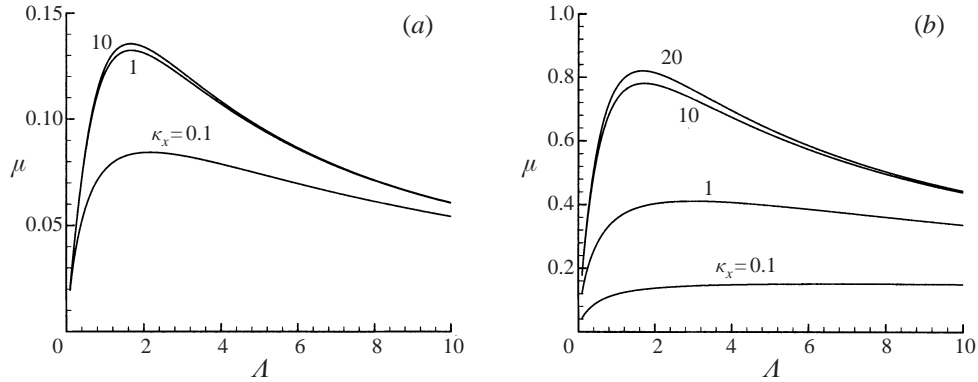


FIGURE 1. Growth rate of the overturning instability versus A : curves for different values of κ_x with (a) $\gamma = 1$ and (b) $\gamma = 10$; $\Delta = 0.3$.

particularized to a step,

$$B(\tilde{x}) = \begin{cases} 1, & \tilde{x} < 0 \\ 1 + \Delta, & \tilde{x} > 0, \end{cases} \quad (3.22)$$

where Δ is constant. We can take the Fourier transform in (3.13)

$$\hat{u}_p(\kappa_x) = \frac{1}{2\pi} \int_{-\infty}^{+\infty} u_p(\tilde{x}) \exp(-i\kappa_x \tilde{x}) d\tilde{x} \quad (3.23)$$

to obtain

$$\mu \{ (i\kappa_x + \mu)(\mu + 1) + \gamma\mu \} (\kappa_x^2 + \kappa_y^2) \hat{u}_p = \frac{\gamma \Delta \kappa_y^2}{2\pi} \int_{-\infty}^{+\infty} \hat{u}_p(\kappa_x) d\kappa_x. \quad (3.24)$$

The solution of the integral equation (3.24) is

$$\hat{u}_p(\kappa_x) = \frac{C}{\mu \{ (i\kappa_x + \mu)(\mu + 1) + \gamma\mu \} (\kappa_x^2 + \kappa_y^2)}, \quad (3.25)$$

where C is a complex constant. The characteristic polynomial of instability is obtained by looking for a non-trivial solution of (3.24), which gives

$$\mu(\mu^2 + (1 + \gamma + \kappa_y)\mu + \kappa_y) = \frac{\gamma \kappa_y \Delta}{2}. \quad (3.26)$$

In the Rayleigh–Taylor limit ($\kappa_y \ll 1$), the characteristic roots are

$$\mu_{1,2} = \pm \left(\frac{\kappa_y \gamma \Delta}{2(1 + \gamma)} \right)^{1/2}, \quad (3.27)$$

$$\mu_3 = -1 - \gamma. \quad (3.28)$$

The necessary condition for these long waves to be unstable is simply $\Delta > 0$. Note that $\mu_{1,2}$ are the eigenvalues given by the Rayleigh–Taylor equation (3.15).

In the short-wavelength limit ($\kappa_y \gg 1$), the roots of (3.26) result in a bounded growth rate

$$\mu_{1,2} = \frac{1}{2} \{ -1 \pm (1 + 2\gamma\Delta)^{1/2} \}, \quad (3.29)$$

$$\mu_3 = -\kappa_y. \quad (3.30)$$

The condition for these short waves to be unstable is also that $\Delta > 0$, in which case

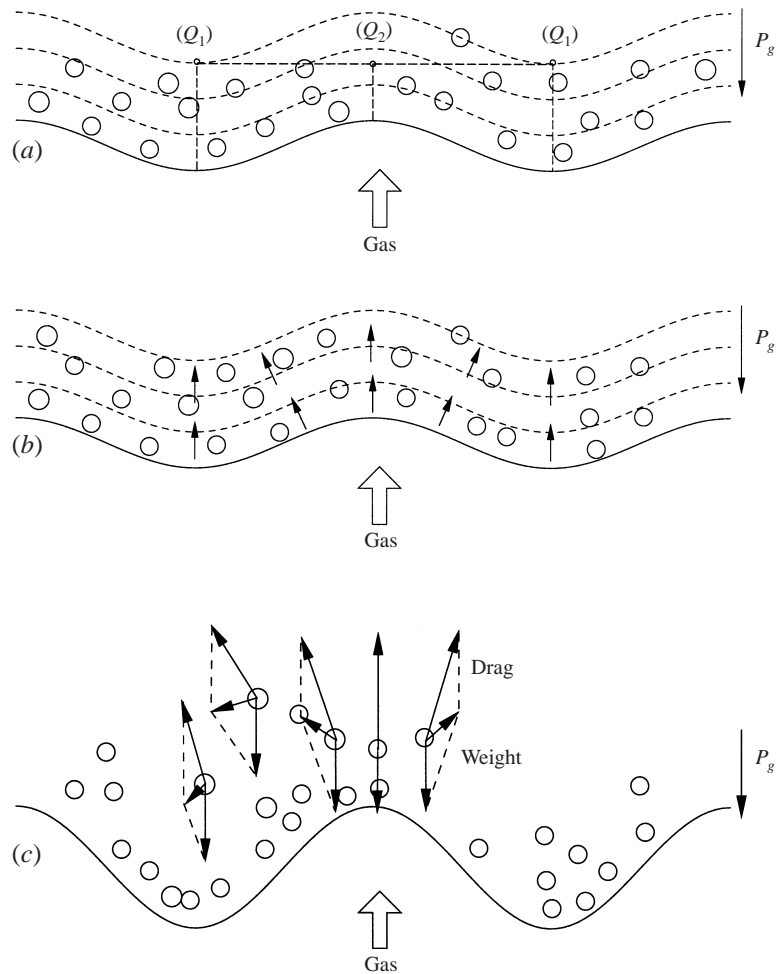


FIGURE 2. Physical mechanism of the overturning instability: (a) loss of pressure in the cloud of particles; (b) movement of gas; (c) drag and weight forces exerted over particles.

$\mu_1 > 0$. It is important to note that while the growth rate of the Rayleigh–Taylor instability described by equation (3.15) is unbounded for high wavenumbers, the growth rate of the instability of the concentration gradients predicted by the dusty gas equations (3.13) is bounded.

To explain the physical mechanism of this instability, we consider in figure 2 a step distribution of particles. This figure has been divided into a sequence of three parts: (a), (b) and (c). In each, particles are found in the upper part of the figure and the gas flow blows from bottom to top. In figure 2(a) particles are at rest with their weight balanced by the drag force exerted by the gas. We initially corrugate the interface that separates particles and gas. Since the pressure drop is proportional to the distance of penetration into the cloud of particles and to the difference between gas and particle velocities, gas pressure at point Q_1 is lower than at Q_2 . Hence, besides the vertical gradient of the gas pressure imposed to suspend the particles, a horizontal gradient appears that creates a movement of gas from Q_2 to Q_1 (figure 2b). This movement of gas exerts a drag force over the particle which has a horizontal component. The

horizontal component of the drag cannot be balanced by their weight and particles begin to move (figure 2c). This movement of particles makes the corrugation more pronounced.

4. Nonlinear evolution of the disturbances

We study the nonlinear evolution of the disturbances by means of a fully spectral numerical simulation of the time-evolving initial value problem defined by the dusty gas equations (2.3)–(2.6). Boundary conditions are considered periodic and the spatial discretization uses Fourier expansions. The convolution sums of the nonlinear terms are calculated via the inverse discrete Fourier transform and the aliasing error is removed in order to have a true spectral Galerkin method. Time integration is accomplished by an explicit fourth-order Runge–Kutta scheme. Further details of the numerical code can be found in Hernández (1990).

All lengths are normalized with the viscous length L_v so that the box lengths L_x and L_y are given in terms of a dimensionless wavenumber $\kappa_x = 2\pi L_v/L_x$ and the aspect ratio $A = L_x/L_y$. The flow repeats periodically outside the numerical box, both laterally (\tilde{y}) and longitudinally (\tilde{x}).

Since the uniform state is stable, the initial condition is taken non-uniform. As an initial condition we take the sinusoidal distribution of particles $B(\tilde{x})$ given in (3.16) and analysed in § 3.2. The particles are considered to be at rest, and their mass fraction is

$$\beta(\tilde{x}, \tilde{y}) = \gamma B(\tilde{x})(1 + \epsilon_y \cos(\kappa_y \tilde{y})), \quad (4.1)$$

where ϵ_y is the amplitude of the transversal perturbation. The mass flux of the mixture is kept constant in time by a pressure field,

$$\tilde{P}_g(\tilde{x}, \tilde{y}, \tilde{t}) = \tilde{P}_0(x) + \tilde{P}(x, y, t), \quad (4.2)$$

where \tilde{P}_0 is chosen using (3.1) and $\tilde{P}(\tilde{x}, \tilde{y}, \tilde{t})$ is periodic in \tilde{x} and \tilde{y} .

In order to cover the range of validity of the dusty gas equations six different numerical simulations are computed: three (figures 3 and 4) for a value of mass fraction $\gamma = 1$ and the other three (figures 5 and 6) for $\gamma = 10$. Since there is no effective viscous stress in the dusty gas equations (2.3)–(2.6), there is no physical mechanism to describe solutions when high gradients are present. Hence, the simulations are aborted when high gradients are formed with the loss of spectral accuracy.

In all simulations the aspect ratio of the numerical box A is determined by the most unstable transversal perturbation for the initial condition, obtained by the linear analysis given in § 3.2 (see figure 1). The initial condition for all of them is a steady solution with $\epsilon_y = 0$, but the transversal perturbations are subjected to the concentration gradient instability. As was shown in § 3.3, those gradients in which the gas blows towards regions of higher concentration tend to corrugate.

The first simulation corresponds to a mass fraction of particles $\gamma = 1$ with $\kappa_x = 1$ and $A = 1.7$. Figure 3 shows plots of the mass fraction of particles β at successively increasing values of the dimensionless time \tilde{t} . A grey-scale has been used, where white stands for the lowest value of β and black for the highest value. Initially particles are at rest suspended by the gas flow. Once the concentration gradient is perturbed with a transversal disturbance, the gas pressure disturbance gives a two-dimensional disturbance to the gas which drags particles laterally and longitudinally. Plots have been shifted in the vertical direction so that entire clusters appear. The first three frames show how the fronts corrugate transversally: in the second frame $\tilde{t} = 21$

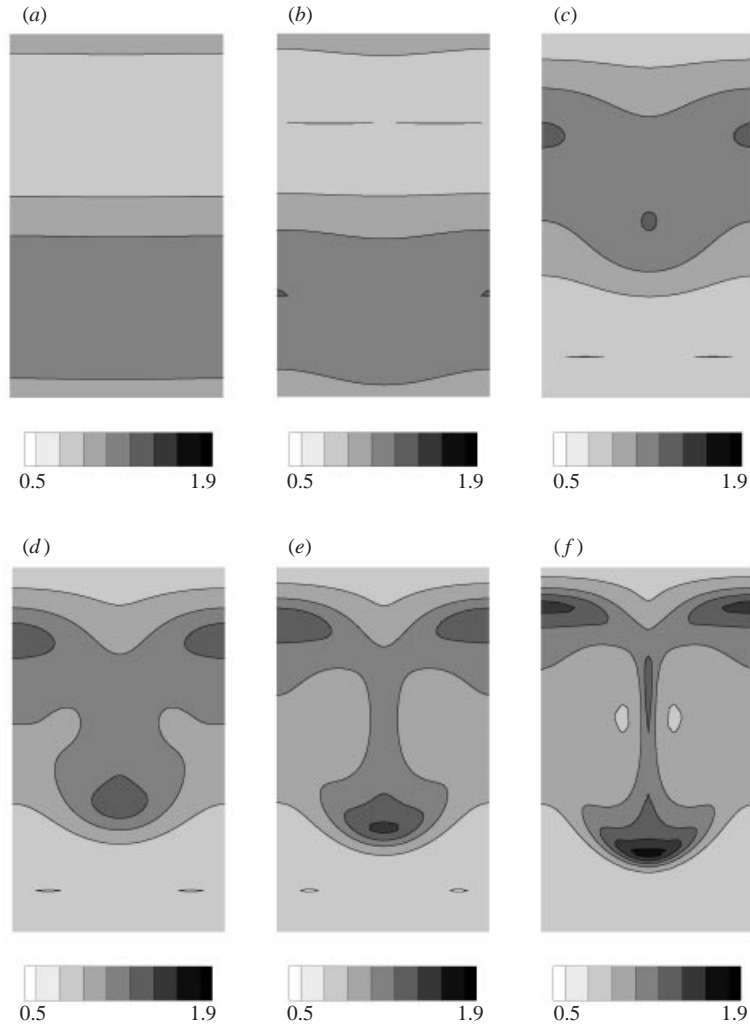


FIGURE 3. Grey-scale plots displaying the evolution of the mass fraction of particles β over the time of the simulation, showing the formation of paraboloids with $\gamma = 1$ and $A = 1.7$. Initial conditions $\kappa_x = 1$, $A = 0.3$ and $\epsilon_y = -0.01$. Resolution 48×48 . (a) Initial condition $\tilde{t} = 0$; (b) $\tilde{t} = 21$; (c) $\tilde{t} = 30$; (d) $\tilde{t} = 36$; (e) $\tilde{t} = 39$; (f) $\tilde{t} = 42$.

(figure 3b) the lower edge of the gradient corrugates, with this distortion progressing in the third frame $\tilde{t} = 30$ (figure 3c). It can be seen in figure 3(e) how the distortion progresses by breaking the front, giving rise to progressively more isolated zones of high particle concentration, which in turn originate a small paraboloid which can be seen in the last frame (figure 3f). These paraboloids are, in fact, particle clusters such as those reported by Glasser *et al.* (1998) to arise from the secondary instability of fluidized beds.

In order to analyse the effect of the characteristic length of the concentration gradient, we represent in figure 4 at a late time three different simulations for $\gamma = 1$ with initial concentration profiles with $\kappa_x = 10, 1, 0.1$. Taking the advantage of left-right symmetry of all figures, the velocity vectors of the gas are superposed on the left of the grey-scale plots, and on the right the velocity vectors of particles are shown.

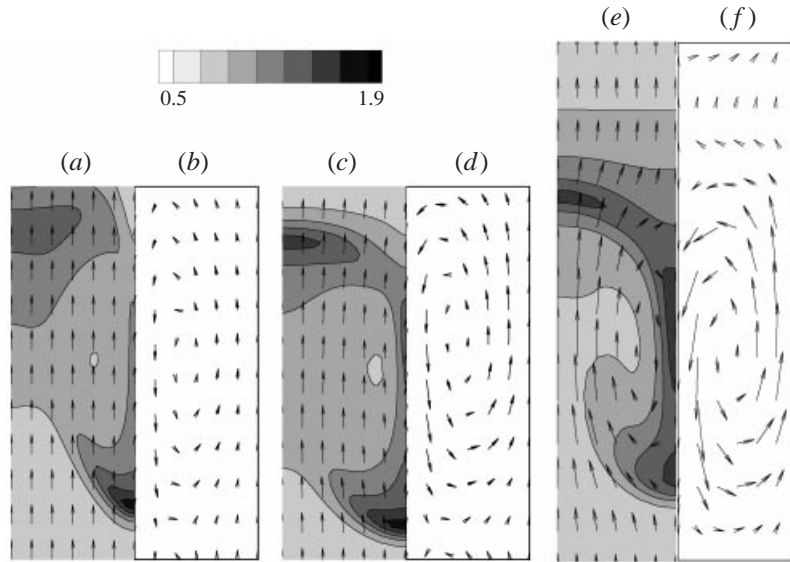


FIGURE 4. Grey-scale plots of mass fraction of particles β and velocity vectors of gas (left) and particles (right) displaying the final structures for different values of κ_x with $\gamma = 1$. Initial conditions $A = 0.3$ and $\epsilon_y = -0.01$. Resolution 48×48 . Velocity vectors of gas are plotted with the same scale. Velocity vectors of particles have different scale factors referred to the gas: (b) 20; (d) 6 and (f) 2. (a, b) Simulation with $\kappa_x = 10$ and $A = 1.7$ at $\tilde{t} = 39$; (c, d) simulation with $\kappa_x = 1$ and $A = 1.7$ at $\tilde{t} = 42$; (e, f) simulation with $\kappa_x = 0.1$ and $A = 2.2$ at $\tilde{t} = 68$.

The frame of reference from which velocity vectors are seen is the laboratory frame. Velocity vectors of the gas are plotted with the same scale. Velocity vectors of particles have different scale factors referred to the gas: (b) 20; (d) 6; (f) 2. While for long characteristic lengths $L_x \gg L_v$ (figure 4e) falling streamers of particles are formed, for $L_x = O(L_v)$ falling and rising paraboloids are observed. Recirculation cells of particles are observed in all simulations (figure 4b, d, f) forming rising and falling paraboloids. For the velocity of the gas, recirculation is observed only in figure 4(e).

The following figures are for suspensions with a characteristic mass fraction $\gamma = 10$. In figure 5 the evolution of the mass fraction of particles β is depicted at successively increasing values of dimensionless time \tilde{t} . In this simulation $\kappa_x = 1$ and $A = 3$. The last three frames ($\tilde{t} = 10, 11, 12$) clearly depict the formation of falling streamers, with particles accumulating in the middle of the cell and with the formation of zones of lower particle concentration.

To study the behaviour of a suspension with varying characteristic length of the concentration gradients, three different simulations ($\kappa_x = 10, 1, 0.1$) are shown in figure 6 with $\gamma = 10$. Velocity vectors of gas and particles are plotted with the same scale factors as figure 4. For small characteristic lengths ($L_x \ll L_v$), falling and rising paraboloids are formed (figure 6a) and for long lengths, falling streamers are observed. Since the mass fraction is greater than in figure 4, the gas velocity is more perturbed by the presence of particles as is observed in figure 6(e). The particle velocity vectors show that the particles accumulate in the middle of the cell, giving rise to the falling streamers. Again, recirculation of gas is observed in figure 6(e).

It is noteworthy that the paraboloid-shaped structures depicted for the mass fraction of particles in figure 4(a) and figure 4(c) clearly resemble those experimentally observed by Horio & Kuroki (1994) for a dilute transport condition.

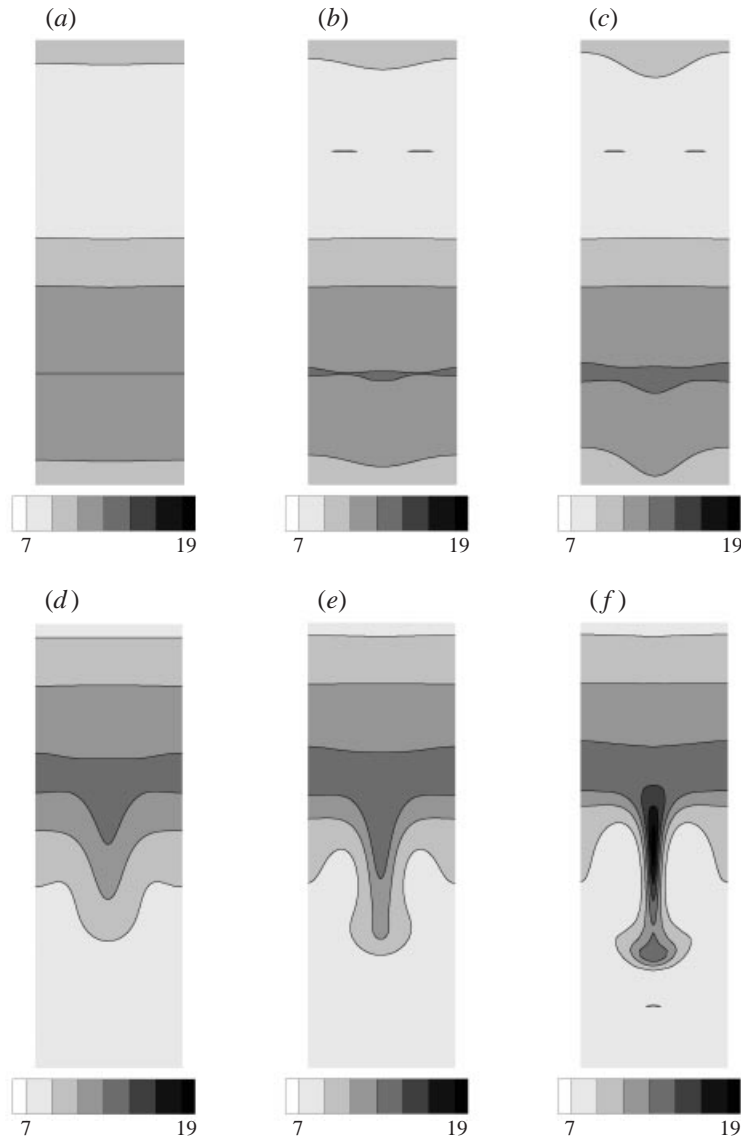


FIGURE 5. Grey-scale plots displaying the evolution of mass fraction of particles β over the time of simulation, showing the formation of falling strands with $\gamma = 10$ and $\mathcal{A} = 3$. Initial conditions $\kappa_x = 1$, $\mathcal{A} = 0.3$ and $\epsilon_y = -0.01$. Resolution 48×48 . (a) Initial condition $\tilde{t} = 0$; (b) $\tilde{t} = 6$; (c) $\tilde{t} = 8$; (d) $\tilde{t} = 10$; (e) $\tilde{t} = 11$; (f) $\tilde{t} = 12$.

5. Conclusions

In this paper we have studied the stability of concentration gradients in dusty gases. It has been demonstrated by a linear analysis of stability that when fronts of characteristic length L_x are blown towards regions of higher concentration of particles, these fronts are unstable to two-dimensional disturbances of characteristic length L_y and the maximum growth rate is achieved at $L_y = O(L_x)$. This instability has been related to the Rayleigh–Taylor one and they are the same in the limit of the viscous length of an isolated particle $L_v \ll L_x$. For these long waves the relaxation

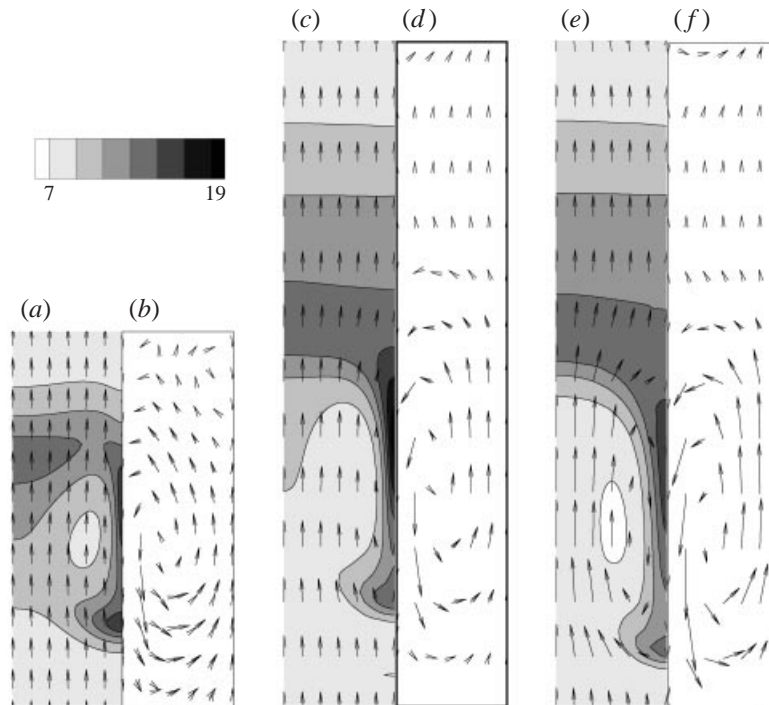


FIGURE 6. Grey-scale plots of mass fraction of particles β and velocity vectors of gas (left) and particles (right) displaying the final structures for different values of κ_x with $\gamma = 10$. Initial conditions $A = 0.3$ and $\epsilon_y = -0.01$. Resolution 48×48 . Velocity vectors of gas are plotted with the same scale. Velocity vectors of particles have different scale factors referred to the gas: (b) 20; (d) 6 and (f) 2. (a, b) Simulation with $\kappa_x = 10$ and $A = 1.7$ at $\tilde{t} = 6$; (c, d) simulation with $\kappa_x = 1$ and $A = 3$ at $\tilde{t} = 12$; (e, f) simulation with $\kappa_x = 0.1$ and $A = 3$ at $\tilde{t} = 30$.

time of an isolated particle is much smaller than the characteristic time of the flow, the particles follow closely the variations of the gas velocity, and the mixture can be considered as one phase with a new density profile determined by the presence of particles. On the other hand, when $L_v = O(L_x)$, the dusty gas cannot be considered as one phase because particles do not follow closely the variations of gas and hence the growth rate of disturbances in this limit is different from the Rayleigh–Taylor ones. It has been demonstrated that the growth rate of this instability is bounded by the relaxation time of an isolated particle.

It has been shown by a fully numerical simulation how this instability corrugates fronts, forming falling streamers and paraboloids depending on the characteristic length of the concentration gradient and the mass fraction of the suspension.

Thanks are given particularly to Professor J. Jiménez for valuable discussions and suggestions on the first drafts of the manuscript. Reading and discussion of the manuscript by Professor M. A. Gañán-Calvo, Dr J. Dávila, Dr C. Lorenzo, Professor I. Parra and M. Zamecnik is also gratefully acknowledged.

REFERENCES

- ANDERSON, K., SUNDARESAN, S. & JACKSON, R. 1995 Instabilities and the formation of bubbles in fluidized beds. *J. Fluid Mech.* **303**, 327–366.

- BATCHELOR, G. K. 1993 Secondary instability of a gas-fluidized bed. *J. Fluid Mech.* **257**, 359–371.
- BATCHELOR, G. K. & NITSCHKE, J. M. 1991 Instability of stationary unbounded stratified fluid. *J. Fluid Mech.* **227**, 357–391.
- BRERETON, C. M. H. & GRACE, J. R. 1993 Microstructural aspects of the behavior of circulating fluidized beds. *Chem. Engng Sci.* **48**, 2565–2572.
- BUYEVICH, YU. A. 1971 Statistical hydromechanics of disperse systems. Part 1. Physical background and general equations. *J. Fluid Mech.* **49**, 489–507.
- CHANDRASEKHAR, S. 1981 The stability of superposed fluids: the Rayleigh–Taylor instability. In *Hydrodynamic and Hydromagnetic Stability*. Dover.
- DASGUPTA, S., JACKSON, R. & SUNDARESAN, S. 1994 Turbulent gas–particle flow in vertical risers. *AIChE J.* **40**, 215–228.
- DREW, D. A. 1983 Mathematical model of two phase flow. *Ann. Rev. Fluid Mech.* **15**, 261–291.
- FANUCCI, J. B., NESS, N. & YEN, R.-H. 1979 On the formation of bubbles in gas-particulate fluidized beds. *J. Fluid Mech.* **94**, 353–368.
- GLASSER, B. J., KEVREKIDIS, I. G. & SUNDARESAN, S. 1996 One and two-dimensional travelling wave solutions in gas-fluidized beds. *J. Fluid Mech.* **306**, 183–221.
- GLASSER, B. J., KEVREKIDIS, I. G. & SUNDARESAN, S. 1997 Fully developed travelling wave solutions and bubble formation in fluidized beds. *J. Fluid Mech.* **334**, 157–188.
- GLASSER, B. J., SUNDARESAN, S. & KEVREKIDIS, I. G. 1998 From bubbles to clusters in fluidized beds. *Phys. Rev. Lett.* **81**, 1849–1852.
- GÖZ, M. F. 1995 Transverse instability of plane wavetrains in gas-fluidized beds. *J. Fluid Mech.* **303**, 55–81.
- HARRIS, S. E. 1996 The growth of periodic waves in gas-fluidized beds. *J. Fluid Mech.* **325**, 261–282.
- HARRIS, S. E. & CRIGHTON, D. G. 1994 Solitons, solitary waves, and voidage disturbances in gas-fluidized beds. *J. Fluid Mech.* **266**, 243–276.
- HERNÁNDEZ, J. A. 1990 Analytical and numerical study of instabilities of two phase flows (in Spanish). PhD Thesis, School of Aeronautics. Madrid.
- HERNÁNDEZ, J. A. & JIMÉNEZ, J. 1991 Bubble formation in dense fluidized beds. In *NATO Advanced Research Workshop on The Global Geometry of Turbulence* (ed. J. Jiménez). Plenum. ISBN 0-306-44014-8.
- HOMSY, G. M., EL-KAISSY, M. M. & DIDWANIA, A. 1980 Instability waves and the origin of bubbles in fluidized beds. Part II. Comparison with theory. *Intl J. Multiphase Flow* **6**, 305–318.
- HORIO, M. & KUROKI, H. 1994 Three-dimensional flow visualization of dilutely dispersed solids in bubbling and circulating fluidized beds. *Chem. Engng Sci.* **49**, 2413–2421.
- ISHII, R. & MATSUHISA, H. 1983 Steady reflection, absorption and transmission of small disturbances by a screen of dusty gas. *J. Fluid Mech.* **130**, 259–277.
- JACKSON, R. 1963 The mechanics of fluidized beds. I. The stability of the state of uniform fluidization. *Trans. Inst. Chem. Engrs* **41**, 13–21.
- JACKSON, R. 1996 Locally averaged equations of motion for a mixture of identical spherical particles and a Newtonian fluid. *Chem. Engng Sci.* **52**, 2457–2469.
- NEEDHAM, D. J. 1986 The existence and stability of quasi-steady periodic voidage waves in a fluidized bed. *Z. Angew. Math. Phys.* **37**, 323–339.
- NEEDHAM, D. J. & MERKIN, J. H. 1983 The propagation of a voidage disturbance in a uniformly fluidized bed. *J. Fluid Mech.* **131**, 427–454.
- SAFFMAN, P. G. 1962 On the stability of laminar flow of a dusty gas. *J. Fluid Mech.* **13**, 120–128.
- YERUSHALMI, J. & CANKURT, N. T. 1978 High-velocity fluid beds. *ChemTech* **9**, 564–572.